

REPORT DOCUMENTATION PAGE

Form Approved
OMB NO. 0704-0188

Public Reporting burden for this collection of information is estimated to average 1 hour per response, including the time for reviewing instructions, searching existing data sources, gathering and maintaining the data needed, and completing and reviewing the collection of information. Send comment regarding this burden estimates or any other aspect of this collection of information, including suggestions for reducing this burden, to Washington Headquarters Services, Directorate for Information Operations and Reports, 1215 Jefferson Davis Highway, Suite 1204, Arlington, VA 22202-4302, and to the Office of Management and Budget, Paperwork Reduction Project (0704-0188) Washington, DC 20503.

1. AGENCY USE ONLY (Leave Blank)	2. REPORT DATE 22 Dec 2004	3. REPORT TYPE AND DATES COVERED Final 1 May 2003 – 30 Sep 2004	
4. TITLE AND SUBTITLE Integrated Wide-Band Milli-meter Wave Imaging System		5. FUNDING NUMBERS G: N00014-03-1-0758	
6. AUTHOR(S) Dennis W. Prather			
7. PERFORMING ORGANIZATION NAME(S) AND ADDRESS(ES) Electrical & Computer Engineering University of Delaware 140 Evans Hall Newark, DE 19716		8. PERFORMING ORGANIZATION REPORT NUMBER ELEG332143-122204	
9. SPONSORING / MONITORING AGENCY NAME(S) AND ADDRESS(ES) Office of Naval Research Ballston Center Tower One 800 North Quincy Street Arlington, VA 22217-5660		10. SPONSORING / MONITORING AGENCY REPORT NUMBER	
11. SUPPLEMENTARY NOTES			
12 a. DISTRIBUTION / AVAILABILITY STATEMENT Approved for public release; distribution unlimited.		12 b. DISTRIBUTION CODE	
13. ABSTRACT (Maximum 200 words) In this project, we developed and demonstrated the design, fabrication, and experimental characterization of a millimeter wave imaging system. To achieve these goals we employed our electromagnetic modeling expertise to design and refine the system specifications. A novel two-element all-diffractive millimeter wave imaging system has been implemented to significantly reduce the overall size and weight of system while maintaining mission criteria. We also set up a new and dedicated mmW characterization and testing system. The new test platform with capability of 3D vector-based near field scanning allows us to fully characterize and simulate mmW radiation. Based on this testing system, the in-house fabricated diffractive mmW lens has been characterized and shown to have diffraction limited performance, which results in a demonstrated capability for mmW imaging. In addition, we investigated two broadband frequency-independent antennas: conical and planar spiral antennas, which offer possible integration into the mmW imaging system. Detailed achievements and progress made during the course of this effort are presented in this report.			
14. SUBJECT TERMS Millimeter wave imaging, diffractive lens, Millimeter wave testing system, Numerical electromagnetic techniques, antenna, all optical detection circuit		15. NUMBER OF PAGES 19	
		16. PRICE CODE	
17. SECURITY CLASSIFICATION OR REPORT UNCLASSIFIED	18. SECURITY CLASSIFICATION ON THIS PAGE UNCLASSIFIED	19. SECURITY CLASSIFICATION OF ABSTRACT UNCLASSIFIED	20. LIMITATION OF ABSTRACT UL

NSN 7540-01-280-5500

Standard Form 298 (Rev.2-89)
Prescribed by ANSI Std. Z39-18
298-102

Integrated Wide-Band Millimeter Wave Imaging System

Table of Contents

1.	INTRODUCTION	2
2.	TECHNICAL ACCOMPLISHMENTS.....	3
2.1.	DIFFRACTIVE MMWS IMAGING SYSTEM.....	4
2.1.1.	Two-diffractive-lens millimeter wave imaging system design.....	5
2.1.2.	Electromagnetic Analysis of Imaging System.....	7
2.1.3.	Fabrication of Diffractive Lens and Experimental Setup	9
2.2.	DESIGN AND ANALYSIS OF BROAD BAND ANTENNA.....	14
2.2.1.	Two-arm Conical Spiral Antenna	14
2.2.2.	Two-arm Planar Spiral Antenna	17
3.	CONCLUSION.....	17

Integrated Wide-Band Millimeter Wave Imaging System

FINAL REPORT

Dennis W. Prather, Ph.D.

University of Delaware
Department of Electrical and Computer Engineering
140 Evans Hall, Room 217B
Newark, DE, 19716-3130
Tel: (302)831-8170, Fax: (302)831-8172, Email: dprather@ee.udel.edu

Abstract

In this project, we developed and demonstrated the design, fabrication, and experimental characterization of an electro-optic millimeter wave imaging system. To achieve these goals we employed our electromagnetic modeling expertise to design and refine the system specifications. A novel two-element all-diffractive millimeter wave imaging system has been implemented to significantly reduce the overall size and weight of system while maintaining mission criteria. We also set up a new and dedicated mmW characterization and testing system, which includes a high-end network analyzer and a new probe station. The new test platform with capability of 3D vector-based near field scanning allows us to fully characterize and simulate mmW radiation. Based on this testing system, the in-house fabricated diffractive MMW lens has been characterized and shown to have diffraction limited performance, which results in a demonstrated capability for mmW imaging. In addition, we investigated two broadband frequency-independent antennas: conical and planar spiral antennas, which offer possible integration into the mmW imaging system. Detailed achievements and progress made during the course of this effort are presented in this report.

1. INTRODUCTION

Millimeter waves (mmWs) are electromagnetic radiation with wavelengths in the range 1 cm to 1 mm (with corresponding frequencies of 30 to 300 GHz), and are located between the microwave and infrared portions of the spectrum. Because of their unique ability to penetrate fog, dust, smoke, and light rain, mmW imaging systems are very attractive in many military applications. However, their use in military systems has been limited due to the lack of suitable technologies to meet and exceed the mission specific design criteria, e.g., resolution, field of view, sensitivity, and cost. While several mmW systems have been built, that serve to demonstrate their utility, they have not been widely used. The main reason for this is that in comparison to optical wavelengths, mmWs are 1,000 to 10,000 times larger, and as a result, the associated imaging elements and corresponding systems tend to be large, expensive, and inconvenient. Especially for military airborne applications, systems realized to date have been impractical. To overcome this problem, this project developed a diffractive imaging system to significantly reduce the size and weight of the whole system while still meeting, and in some cases exceeding, mission specific design criteria.

A Diffractive Optical Elements (DOE) contains a wavelength scale surface relief which guides and redirects incident radiation by virtue of mutual interference. In conventional optical systems, the wavelength scale of diffractive optical elements, on order of several hundreds of nanometers, leads to challenges in fabrication. However, for millimeter wave imaging systems, since the minimum feature size is on the order of millimeters, it is much easier to machine the corresponding DOE devices using modern machining technology. To this end, one of the more challenging aspects in this project was to design an all-diffractive system the maintained aberration control. While aberration theory has been studied for more than a century most of the work done to date has been focused on geometrical optics and relatively few on the aberration theory of diffraction. Almost all current optical design software has been developed based on geometrical optics, in which case they are not ideally suited for systems that contain diffractive lenses. For this reason, we developed our own analysis code to design and optimize millimeter wave all-diffractive imaging systems. In addition to developing ultra-lightweight imaging elements and systems we also concentrated on developing an alternative approach to sensing mmW radiation, namely a new type of mmW focal plane array.

As the millimeter wave approaches higher frequencies, conventional all electronic high-speed detection and read out circuits, monolithic-microwave-integrated-circuits (MMICs), which implement the filtering, amplification, and mixing operations, become increasingly more expensive. In addition, approaches based on antenna-coupled microbolometers have proven to have noise-equivalent-powers (NEP) in tens of picowatts, which do not satisfy sensitivity requirements in many mission related applications. To overcome these limitations this effort is focused on developing an all-optical read out imager for MMWs. This alternative approach does not require expensive high-speed electronic detection and read out microwave circuits. In addition, this technology allows, in principle, to extend into sub-millimeter and even the Terahertz region. Moreover, the all-optical read out approach can achieve a NEP down to tens of femtowatts by exploiting the inherent electro-optic properties of GaAs nano-scale waveguide and by leveraging the tremendous effort that has been expended by the telecommunications industry in high-Q multiplexing. To this the end, the mmW signals can be converted into 100 GHz sidebands on an optical carrier. The mmW energy can then be detected after filtering the optical carrier. In addition, our approach will afford economies-of-scale being that it is completely compatible with planar/wafer-scale fabrication processes.

In our mmW imaging system, the antenna is a device designed for picking up the millimeter wave radiation. The modulator is placed at the point of where antenna produces a maximum in the RF field, where maximum modulation will take place. Optimal design of antenna is particularly important from sensitivity and efficiency points of view, which means that a well designed passive antenna will significantly improve overall system performance. To this end, two antennas are taken into account in this project effort. In the remainder of this report we present the details of our achievements.

2. TECHNICAL ACCOMPLISHMENTS

The key technical focus of this effort is to develop millimeter wave imaging system, which includes a millimeter wave diffractive lens system, all-optical mmW detection and read out circuit, and their associated devices.

To this end, we first present our theoretical investigation of the mmW imaging system made of the diffractive optical elements. Due to the wavelength scale features of DOEs, rigorous numerical electromagnetic techniques are required to take into account the electromagnetic couplings and interactions. Various numerical methods, such as Finite-difference and Time-domain (FDTD) method and

plane wave spectrum method, are employed to accurately evaluate the performance of imaging the system. A novel two-element all-diffractive millimeter wave imaging system has been proposed. This design significantly reduces the overall size and weight of system while sufficiently meets and even exceeds the military mission specifications.

On other hand, to experimentally characterize the designed mmW imaging system, we set up an mmW test facility, which includes a network analyzer, with a test and measurement capability spanning 45MHz through 110GHz, and a probe station. The new test platform has capability of 3D vector-based near field scanning and allows us to fully characterize and simulate mmW radiation.

Another key device in our mmW imaging system is the receiving antenna, which has also been investigated in this effort. To this end, two broadband antennas, conical and planar spiral antennas, are proposed. Ultimately, they will be integrated into our modulator system, which is the focus of the follow on effort, currently underway. The remainder of this report describes accomplishments in each area of the overall effort.

2.1. DIFFRACTIVE MMWS IMAGING SYSTEM

A diffractive lens is an optical element that redirects light through the propagation and mutual interference of a wavefront, in comparison to the more conventional methods of refraction and reflection. Accordingly, a diffractive lens consists of a surface relief structure with many features of different size on its surface. Each feature can be utilized to optimize aberration control and, thus, offer a more complete set of design freedoms, which enable the realization of efficient imaging systems with only small number of optical elements. In addition, they are also well suited to other nonconventional functionalities, such as off-axis focusing and beam splitting, which can be incorporated into the design of the surface relief diffractive profile. One more significant advantage of using diffractive structures as imaging optics is that their maximum relief heights are equal to $\lambda/(n-1)$, where λ is the design wavelength in free space and n is the refractive index of material. Therefore, it turns out the significant reduction of size and weight of imaging system. For instance, consider a diffractive lens made of Rexolite 1422 (with relative permittivity of 2.53 and density of 1.05 g/cm^3) designed at wavelength of 3.4 mm with focal length and aperture of 200λ , respectively; it has a maximum relief height of 5.76 mm and a weight of 2.28 lbs. However, for a corresponding refractive lens, it would have a thickness of 80.24mm (23.6λ) and weigh 33.2lbs, which is 15 times heavier than a corresponding diffractive lens. Clearly, the bigger the lens the more the reduction will be.

To address the design of the diffractive lenses, one must consider that they contain diffractive features approaching the wavelength of illumination and as a result require rigorous electromagnetic analysis in evaluating lens performance. However, most current optical design software packages are based on geometrical optical design and they do not incorporate the ability for such rigorous analysis. Instead, they typically include a relatively simple scalar based diffraction analysis which limits the features of the elements in the imaging system. The end result here, is that we first needed to create a set of tools for the design and analysis of the diffractive elements in the context of an imaging system. Our approach to this aspect of the project is addressed below.

In this section of the report we present the design, electromagnetic analysis of a two diffractive lens millimeter wave imaging system with wide Field Of View (FOV) of $\pm 15^\circ$ and high resolution. This system consists of two 16-level millimeter wave diffractive lenses with the stop in contact with the first

lens. By applying the Seidel aberrations for a single diffractive lens and the stop shift formula when the stop is not in contact with the lens, we establish the expressions for third-order (Seidel) wave aberrations for this two-lens millimeter imaging system. By setting all Seidel aberrations to zero, an optimal two-lens system that totally compensating all Seidel aberrations has been obtained. In order to accurately evaluate the performance of the system, we have developed a four-step rigorous electromagnetic analysis procedure, which combine FDTD technique and VPWS together to reduce the computational cost and meanwhile efficiently and accurately access the performance of the designed system. Below we provided the detailed design procedure and then we present the four-step electromagnetic analysis procedure and its resulting system performance.

2.1.1. Two-diffractive-lens millimeter wave imaging system design

In this section, we present the design of a two element diffractive lens millimeter wave imaging system with a FOV of $\pm 15^\circ$ and high resolution. The system is illustrated as in Figure 1. Although the method of using multiple diffractive lenses to compensate for aberrations and the primary aberration coefficients for diffractive lenses is well known and has been applied by many authors in their respective applications, we needed applied this fundamental knowledge to establish the expressions for entire system in order to obtain the optimal configuration for our millimeter wave imaging system, which required a large FOV and high resolution. As such, we start from a two principal ray tracing approach to briefly illustrate how we obtain the physical configuration for our millimeter wave imaging system, which meets design requirements by applying fundamental optical imaging formulas, aberration expressions for single diffractive lens with stop in contact and stop shift formula when stop is not in contact with the lens.

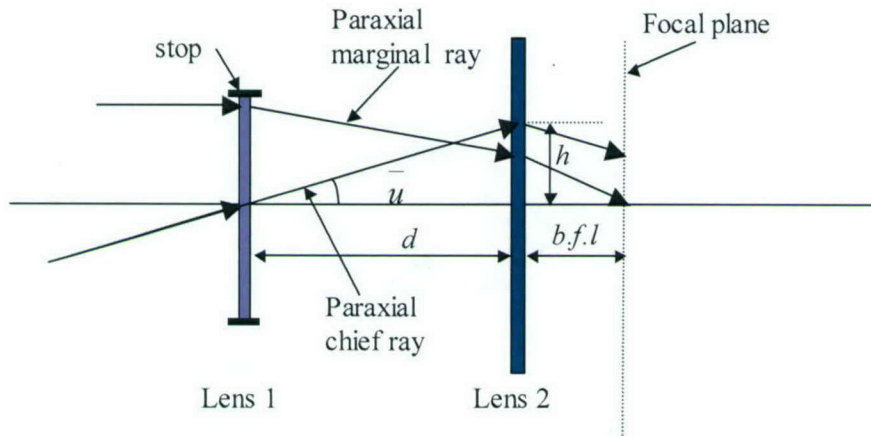


Figure 1. Scheme of two diffractive lens millimeter wave imaging system.

In Figure 1, h is the height at which the Paraxial marginal ray incident on the Lens 2, \bar{u} is the angle at which the Paraxial chief ray is leaving from Lens 1, d is the distance between Lens 1 and Lens 2, and $b.f.l.$ is the back focal length of the complete imaging system. By combining the Seidel coefficients for each lens with the stop shift formula, we can obtain the primary Seidel coefficients $S_1 - S_5$ for the complete system as follows:

$$\begin{cases} S_1 = h^4 \left\{ \phi_1^3 - 8G_1 + (1-d\phi_1)^4 \left[\frac{\phi_2^3}{4} (1+3C_2^2) - 8G_2 \right] \right\} \\ S_2 = \bar{u}h^3 \left\{ -\phi_1^2 + (1-d\phi_1)^2 \phi_2^2 C_2 + d((1-d\phi_1)^3 \left[\frac{\phi_2^3}{4} (1+3C_2^2) - 8G_2 \right] \right\} \\ S_3 = \bar{u}^2 h^2 \left\{ \phi_1 + \phi_2 + 2d(1-d\phi_1) \phi_2^2 C_2 + d^2(1-d\phi_1)^2 \left[\frac{\phi_2^3}{4} (1+3C_2^2) - 8G_2 \right] \right\} f \\ S_4 = 0 \\ S_5 = \bar{u}^3 h \left\{ 3\phi_2 + 3d(1-d\phi_1) \phi_2^2 C_2 + d^2(1-d\phi_1)^2 \left[\frac{\phi_2^3}{4} (1+3C_2^2) - 8G_2 \right] \right\}, \end{cases} \quad (1)$$

where $\phi_i (i=1,2)$ is the lens power, C_i and $G_i (i=1,2)$ are conjugate parameters and aspherical coefficients of the lenses, respectively.

By setting Seidel coefficients to zero and solving this system of equations, the solution for completely compensating for all primary aberrations was obtained:

$$\begin{cases} d = 1.1848F \\ f_1 = 2.53218F \\ f_2 = 0.87943F \\ G_1 = 0.063833/F^3 \\ G_2 = 0.078256/F^3 \\ b.f.l = 0.5321F, \end{cases} \quad (2)$$

where F is the system effective focal length. In this case, if the design wavelength is $\lambda = 3.4mm$, diameter of the first Lens is $D_1 = 0.3m$, diameter of the second Lens is $D_2 = 1.5D_1 = 0.45m$, and the effective focal length of the system is $F = 0.405m$, then the corresponding other design parameters are: the distance between two Lenses is $d = 0.48m$, the back focal length of the system $b.f.l = 0.2155m$. For the first Lens, the focal length $f_1 = 1.0255m$, $f/\# = 3.4183$, aspherical coefficient $G_1 = 0.9609m^{-3}$. For the second Lens, the focal Length $f_2 = 0.3562m$, $f/\# = 0.8$, aspherical coefficient $G_2 = 1.1780m^{-3}$. Once the aspherical coefficient and Lens focus is known, if neglecting the high order term, the diffractive Lens pattern can be determined by

$$f_i(x) = \frac{\text{int}\left(\frac{(Nlev-1) \text{mod}(Ax^2 + G_i x^4, \lambda)}{\lambda}\right)}{Nlev} \frac{\lambda}{n-1} \quad (3)$$

where $A = -\frac{1}{2f}$, f is the Lens focus, $Nlev$ is the number of the quantized levels, and n is the refractive

index of the material made of diffractive Lens. Thus far, we designed a two diffractive lens millimeter wave imaging system, which totally compensates all primary monochromatic aberrations. In the next analysis section, we will propose a four-step electromagnetic analysis model to accurately show high performance of this system.

2.1.2. Electromagnetic Analysis of Imaging System

According to the system configuration given in the design section, the second diffractive lens in the proposed two-diffractive-lens millimeter wave imaging system has a diameter of 132.4λ and $f/\#$ of 0.8. According to reference, this diffractive lens is far beyond the scalar region. This implies that the coupling effects between electromagnetic field components are very strong in this case and cannot be ignored. As such, rigorous electromagnetic analysis model is required to accurately evaluate the performance of the system. In order to save computational cost and enabling electromagnetic analysis of such a large system, we proposed a four-step electromagnetic analysis model. In this model, we combine two well-known electromagnetic techniques and use a four-step analysis process to perform a rigorous system simulation. The first technique we used in our analysis is the Finite-Difference Time-Domain (FDTD) method. The second technique is based on the Vector Plane-Wave Spectrum (VPWS) propagation method. The VPWS method is an efficient technique for the propagation of EM waves. Its efficiency lies in the ability to propagate EM waves from one plane to another using Fast Fourier Transforms (FFTs). The four-step analysis scheme is illustrated in Figure 2.

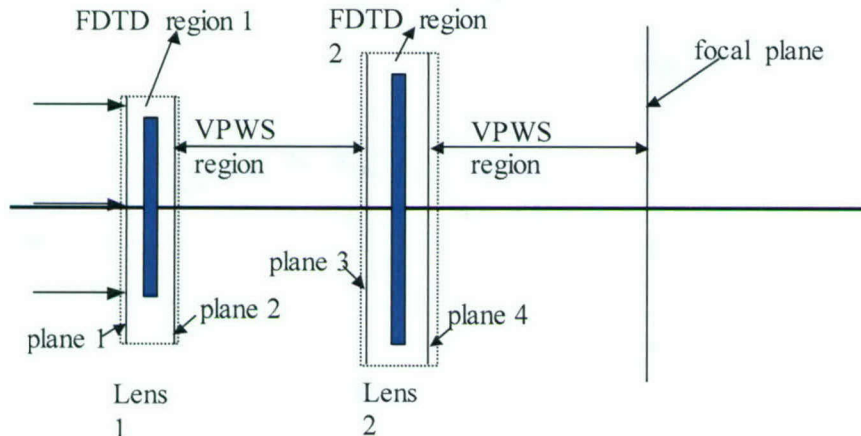


Figure 2. Electromagnetic analysis model of the two diffractive lens millimeter wave imaging system.

In Figure 2 the regions surrounded by the dotted lines are FDTD computational regions and Planes 1, 2, 3 and 4 are taken from inside the computational regions as output planes and input planes of FDTD calculation. Input planes are where we implement excitation for FDTD calculation. Output planes are where we take fields as input of VPWS to propagate to the image plane. The region between plane 2 and plane 3 and the region between plane 4 and image, or focal, plane are the VPWS regions for rigorous electromagnetic wave propagation. In this four-step analysis, the FDTD is used to solve the EM boundary value problem without approximation to obtain the near-field distribution and the VPWS method is applied to propagate the near-fields to the plane of observation so that in each FDTD calculation, we can set the computational region just beyond one of diffractive lens and thus significantly save computational cost.

In the case where all of the diffractive lenses are cylindrical, 2-Dimensional (2D) simulation is required to evaluate the system performance. In other words, when we apply the four step electromagnetic analysis model discussed above to accurately access the image quality, i.e., to calculate the diffraction efficiencies,

we use 2D FDTD in near field calculations for each diffractive lenses and use 2D Fast Fourier Transform (FFT) to propagate each field components from one plane to another plane. Since our millimeter wave imaging system requires a FOV of $\pm 15^\circ$, to show the system performance over the required FOV, we choose four separate incident angles, $\theta_1 = 0^\circ$, $\theta_2 = 5^\circ$, $\theta_3 = 10^\circ$ and $\theta_4 = 15^\circ$ to calculate the diffraction efficiency for each. Figure 3 shows the performance of the two diffractive lens millimeter wave imaging system described in the design section. In the propagation plots, the white line indicates the focal plane, and horizontal axis represents the dimension perpendicular to the optical axis, where zero is where the optical axis is located. The vertical axis represents the distance from the second diffractive lens. Figure 3 (a), (b), (c) and (d) are propagation plots of field intensity for normal incidence and 5, 10 and 15 degrees, respectively. The diffraction efficiencies under these four different incidences are 82.34%, 79.2%, 69.97% and 59.1%, respectively.

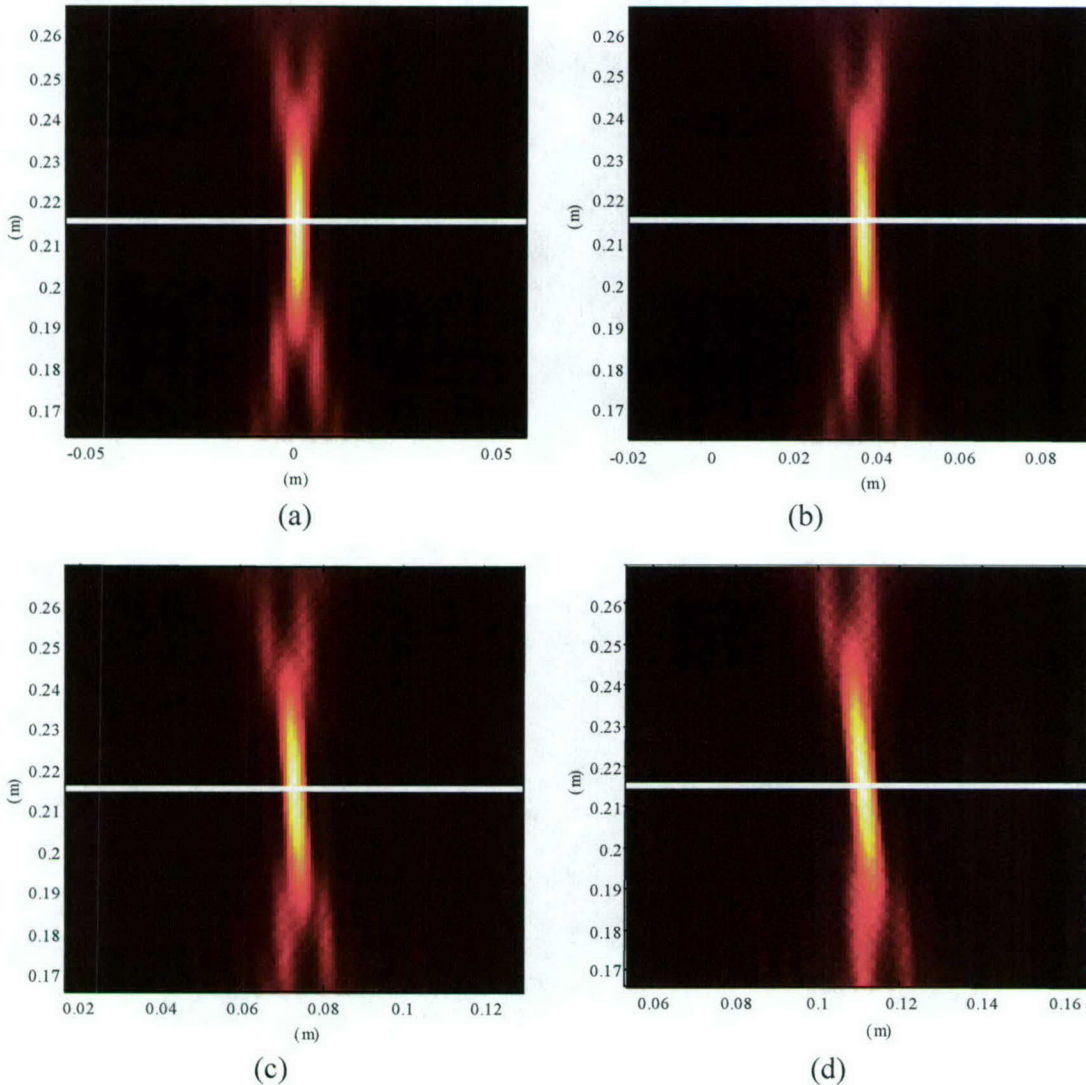


Figure 3. Two dimensional plot of intensity for different incident angles of (a) normal incident, (b) 5° , (c) 10° , and (d) 15° .

In the case when the diffractive lenses are axially symmetric, full three-dimensional (3D) electromagnetic simulation is required to evaluate the system performance. In this case, we applied our four-step electromagnetic analysis model to evaluate system performance but used a full 3D FDTD model in near field calculations for each diffractive lens. However, since the lens profiles are axially symmetric, we can employ an axially symmetric, or Body Of Revolution (BOR), formulation of FDTD in this case. BOR FDTD incorporates the axial symmetry of diffractive lens into the FDTD method to dramatically reduce a full 3D to a 2D problem, which thus reduces the FDTD computational cost by orders of magnitude. Once the near fields are obtained using BOR FDTD, we propagate them to the plane of interest using an axially symmetric formulation of the plane wave spectrum technique, named as Vector Plane Wave Spectrum (VPWS). Figure 4(a) and (b) show the image of field intensity on the focal plane, line scans of field intensity along 0° and 90° on the focal plane for the two-diffractive-lens millimeter wave imaging system described in the design section for normal incidence when both diffractive lenses are axially symmetric. The four-step electromagnetic analysis, which combines BOR FDTD and VPWS together, gives a diffraction efficiency of 81.09% in this case.

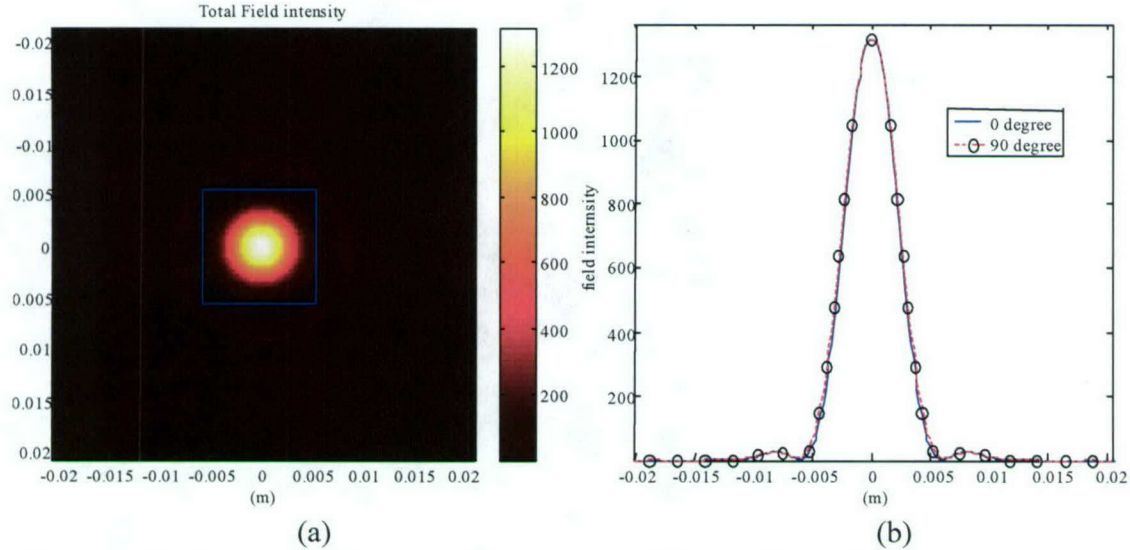


Figure 4. Performance of the two-axially-symmetric-diffractive-lens millimeter wave imaging system for normal incidence. (a) The image of field intensity on focal plane, and (b) line scans of field intensity on focal plane.

2.1.3. Fabrication of Diffractive Lens and Experimental Setup

In this project we used Rexolite slabs to fabricate the mmW diffractive lenses. Rexolite is a plastic-like material with low loss and refractive index $n= 1.59$ when working at mmW regime. As mentioned in the last section, the thickness of the lenses is designed to be $\lambda/(n-1)$, which according to scale diffraction theory produces a phase of 2π .

In the millimeter wave regime, this corresponds to a feature size in the diffractive lens on the order of few millimeters, which is within the capability of modern fabrication tools. In this case, a CNC router is employed to fabricate the desired device. The design layout is done using Auto-CAD software and since

the feature sizes of lenses are dependent on the operating wavelength different fabrication precision is required to fabricate lenses for different wavelengths. For example, we use a 1.6 mm router bit to fabricate a 45GHz diffractive lens with focal length f of 150mm . When the radius increases every 1mm , we machine a circle on the lens with the designed depth. By this method, each zone is composed of 16 or more levels. The thickness of the lens is squeezed to only 14mm , while the aperture can be 240mm , containing 5 zones, as shown in Figure 5.



Figure 5. MMW lens fabricated by CNC router machine.

To characterize the lens, we built a mmW imaging system, as shown in Figure 6, based on an Agilent 85106D network analyzer, which encompasses a test and measurement capability spanning 45MHz through 110GHz . The source is launched by a horn antenna ($\Phi=300\text{mm}$), which is connected to the vector network analyzer. In this case, the detector used is a monopole (or named skirt dipole) antenna fed back to the network analyzer. The detector is mounted on an $X-Y$ robot to map the electric field of the mmW profile. In our setup, an XYZ stage is used to provide maximal capability to detect the spatial field distribution along a line-scan, or on a plane or even in a 3D volume space. It is worth noting that in our experiment, we have to make sure that the monopole orientation coincides with the source polarization of interest.

Before we characterized the performance of our millimeter wave diffractive lens, we removed the lens to check and calibrate the source. To do so, we moved the detector close to the horn, selected the suitable frequency, namely 45GHz , and used the motorized stage to automatically control the monopole and scan the local field distribution in the XY plane. The output field distribution of the horn antenna was then mapped, as shown in Figure 7. From the figure, we can see that both amplitude and the phase of the output are quite uniform, which means that the output of mmW source can be approximately looked at as a plane wave. This is the prerequisite for the next step, since the lens is designed based on an incident collimated plane wave.

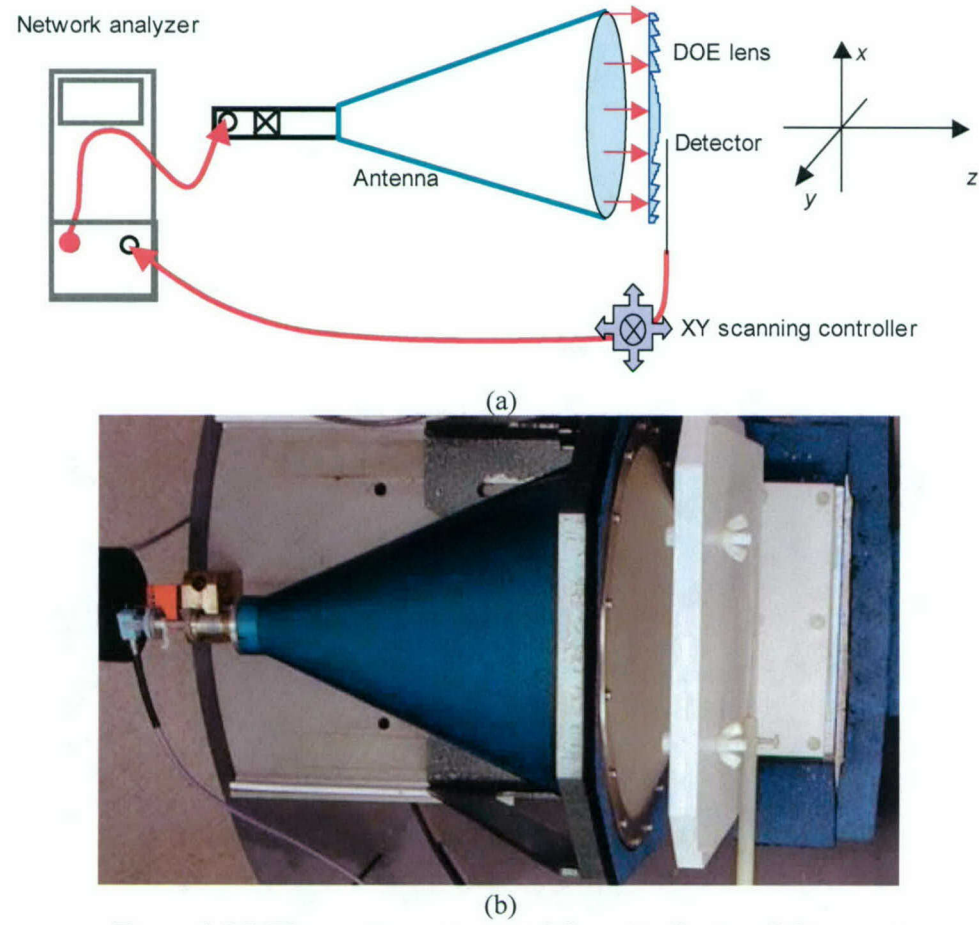


Figure 6. MMW scanning system. (a) Schematic chart, and (b) our setup.

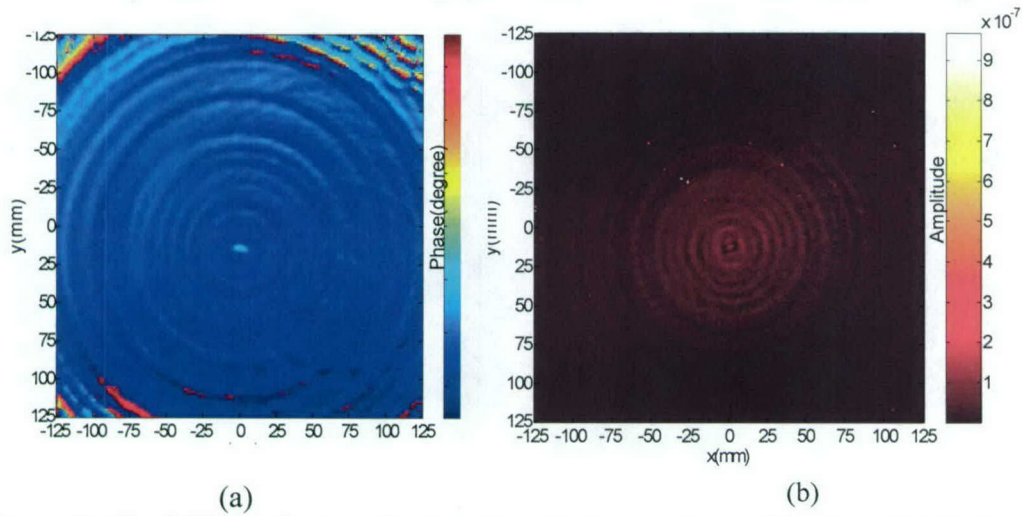


Figure 7. The field distribution of output from the horn antenna. (a) Phase distribution and (b) amplitude distribution.

Next, we inserted the diffractive lens back between the horn and the detector, and mapped the field distribution again. In this case, the detector is very close to the surface of the lens, e.g. 13mm away from. Thus, the field distribution can be treated as the lens transmission function. In addition, from this near field distribution as shown in Figure 8, we mathematically reconstructed a series of near field distribution slices based on Fourier optics theory, e.g., the plane wave angular spectrum method. According to the propagated field distribution, which are propagating away from the surface of diffractive mmW lens, we located the focal position and found that the focal plane is at 136mm from the measured plane. Therefore, the measured focal plane from the surface of lens occurs at $136\text{mm}+13\text{mm}=149\text{mm}$. Our measurements found the actual focal length to be almost exactly same as the design the focal length, which is 150mm.

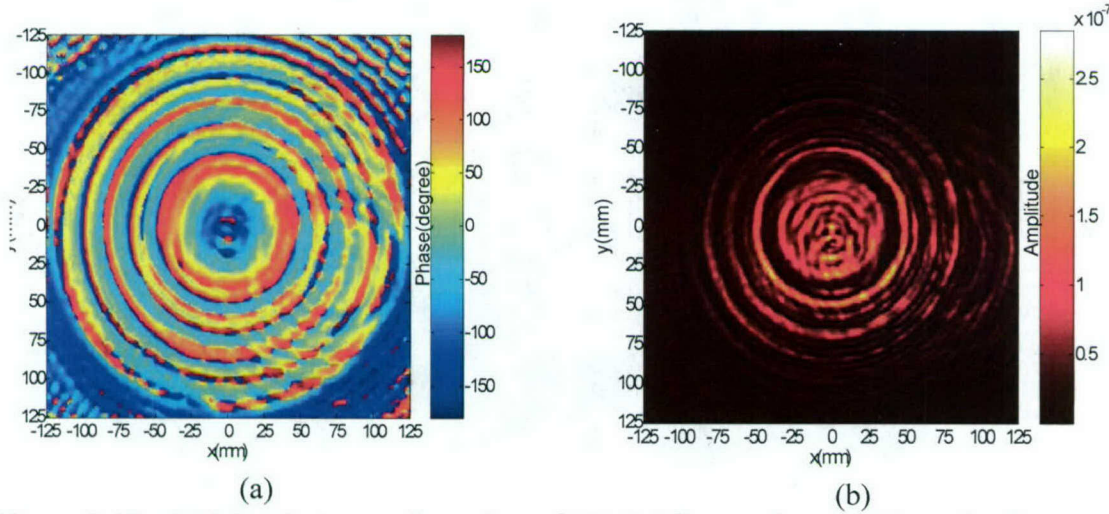


Figure 8. The field distribution on the surface of MMW diffractive lens. (a) Phase distribution and (b) amplitude distribution.

In addition to applying numerical methods to propagate the measured fields along the direction perpendicular to the optical axis, we used our XYZ stages to measure the field distribution. We moved our detector to that expected position, which is 136mm away the initial plane. The measured point-spread function (PSF) is shown in Figure 9. From diffraction theory, the spot size of lens can be determined as $2.44\lambda f/D=13.8\text{mm}$. And using the distribution of PSF, we verified that the performance of the diffractive lens is in fact ideal: by this we mean that the measure point size is very close to the theoretical value and focal length is only slightly smaller than the designed value.

Lastly, we used our diffractive lens in a $2f$ mmW imaging system. To demonstrate the mmW imaging, we made "H" shape in the aluminum sheet and sandwiched the letter between two paper cardboards, which is used as an object of the imaging system. We installed the object on the optical bench, illuminated the object by mmW, placed the lens at $2f$ from the object, adjusted the imaging system, switched to our detector, and scanned the field distribution at $2f$ from the lens. As we expected, we obtained a quite clear image of this letter as shown in Figure 10. This, in turn, proved the capability of the diffractive lens.

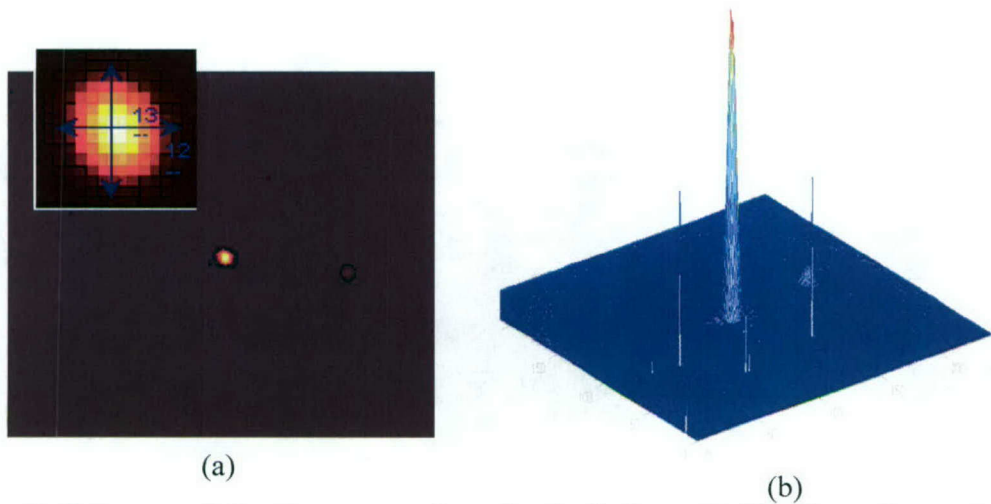


Figure 9. Point spread function measured on the focal plane. (a) 2D plot and zoom-in field distribution, and (b) 3D plot.

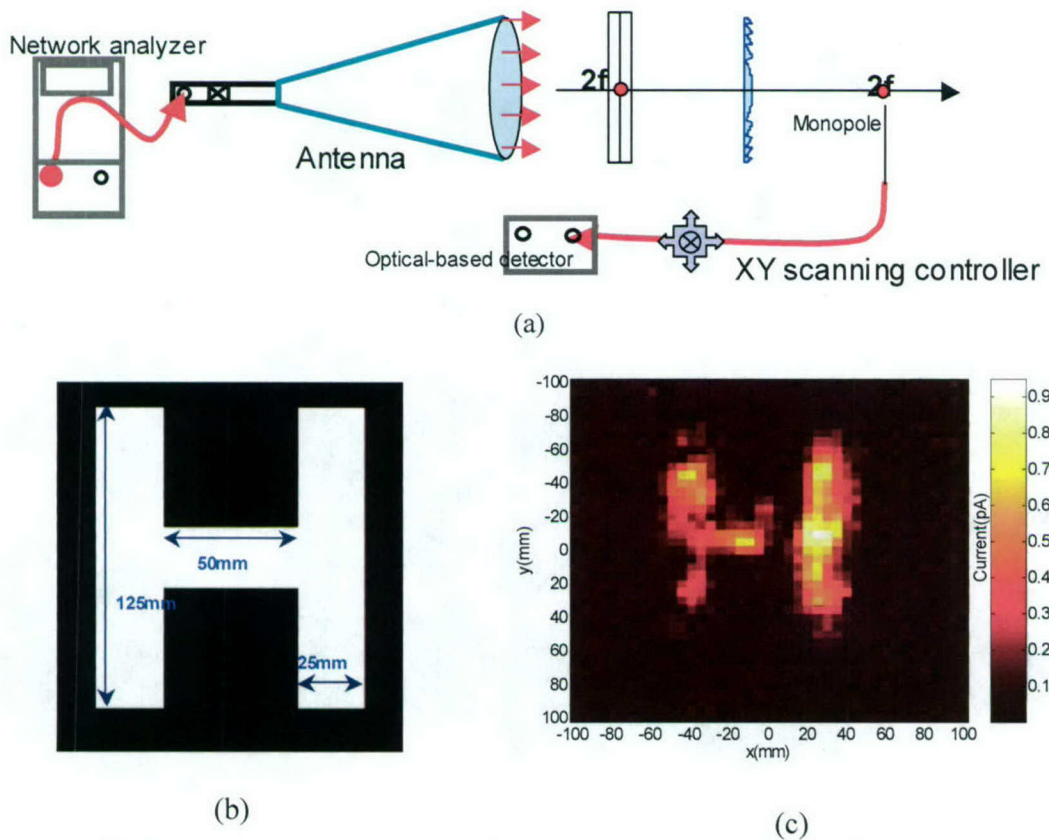


Figure 10. The MMW imaging of an actual object: (a) Schematic chart of 4-f imaging system, (b) an aluminum letter "H", and (c) scanned intensity on the image plane.

2.2. DESIGN AND ANALYSIS OF BROAD BAND ANTENNA

The antenna is designed to sense millimeter wave radiation. The modulator is placed at the point of where antenna produces a maximum in the RF field, analogous to the location of an open in a transmission line. The electro-optic response of the GaAs is extremely fast and capable of THz modulation. For a $100\mu m$ long modulator, the modulator becomes a traveling wave structure for RF frequencies on the order of 500GHz in GaAs. At frequencies approaching 500GHz care has to be taken in the design of the modulator so that optical wave velocity is matched to the RF wave velocity in the modulator structure. These structures can be designed by careful considerations of the antenna design and the electrode pattern on the optical modulator.

To maximally receive the millimeter wave signal, significant effort was made to widely exploit the antenna selection and design. In this project, two antenna configurations were considered, which offer extremely broad bandwidth and relatively high gain. In the following section we discuss these two antenna configurations: conical spiral and planar spiral antennas. To accurately characterize the antenna performances, a rigorous numerical technique, namely 3D FDTD method, is employed.

2.2.1. Two-arm Conical Spiral Antenna

Planar and conical spiral antennas are among the most popular broadband antennas. The genesis of these antennas was in the work of Rumsey during the 1950s, where he introduced two necessary conditions for practical frequency-independent antennas of this type: the angle principle and truncation principle. Briefly stated, the angle principle says that the performance of an antenna that is defined entirely by angles will be frequency independent. Antennas defined entirely by angles are infinite in size, so an additional consideration is required for practical antennas. The truncation principle says that an antenna must have an “active region” of finite size that is responsible for the radiation at a particular frequency. As a frequency is changed, the “active region” moves on the antenna in such a way that the dimensions of this region, expressed in terms of the wavelength, remain constant; hence, the performance remains constant. The antenna is then practically frequency independent over the range of frequencies (bandwidth) for which the active region is completely contained within the finite structure of the antenna.

The two-arm conical spiral antenna, as shown in Figure 11, which is based on Rumsey’s principle and was first proposed by Dyson in 1959. The antenna is constructed by winding two metallic strips around the surface of a truncated cone. Three angles define the geometry of frequency-independent conical spiral antenna. There are the half angle of the cone θ , the wrap angle α , and the angular width of the arm δ . The half angle is measured between symmetry axis and the side of cone. When θ is small, the radiation from the conical spiral antenna is predominantly along the axis of cone. While $\theta = 90^\circ$, the conical spiral antenna becomes a planar spiral, which radiates equally in two directions. δ defines the constant angular width of the arms everywhere along the cone. The most common configuration is that for which $\delta = 90^\circ$.

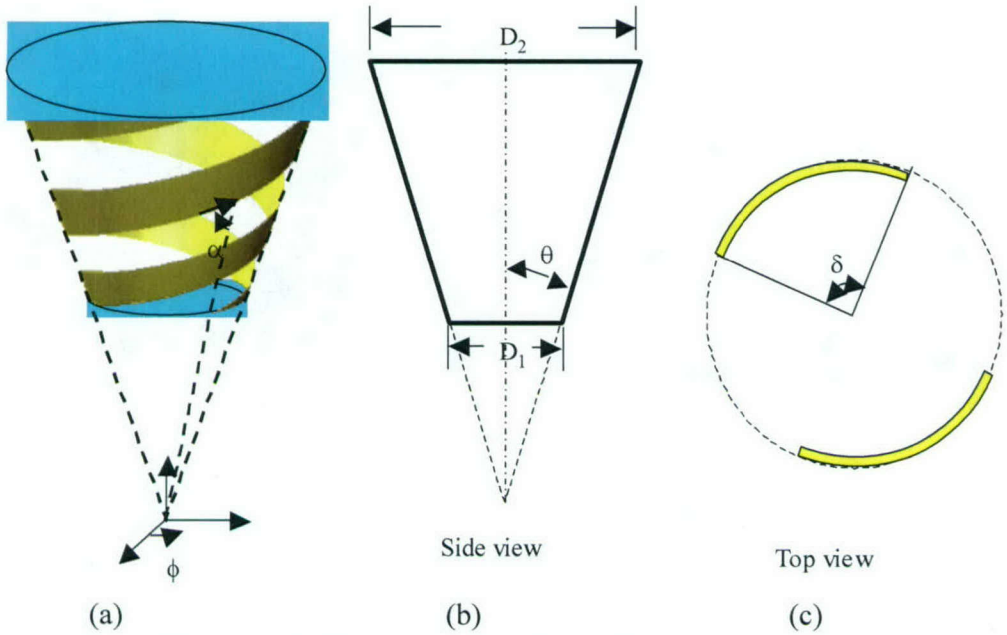


Figure 11. (a) Geometry for the two-arm conical spiral antenna, (b) side view of the basic cone, and (c) top view of the cross section.

The boundaries of the arms for the two-arm conical spiral antenna can be described mathematically with expressions for the radial distance, r , from the apex to a point on the conical surface. From the figure, r_1 describes the distance from the apex of the cone to one boundary of the first arm, and r_1' describes the distance from the apex to the other boundary of the same arm, i.e.,

$$\begin{cases} r_1(\phi) = r_d e^{b|\phi|}, & |\phi| \geq 0 \\ r_1'(\phi) = r_d e^{b(|\phi|-\delta)}, & |\phi| \geq 0 \end{cases} \quad (4)$$

where, b is defined as $b = \sin \theta / \tan \alpha$, and $r_d = D_1 / (2 \sin \theta)$ is the radial distance from the apex to the smaller end of the cone. Note that the magnitude of ϕ is not limited to 2π . The two arms are symmetric to the z axis (diametrically opposite), so the boundaries of the second arm can be obtained by rotating the boundaries of the first arm by the angle π .

The radiation from the well-designed conical spiral antenna is maximum in the direction of the z axis, and in this direction, the electric field is predominantly circularly polarized. The sense of circular polarization, right-handed or left-handed, is determined by the direction in which the arms are wound around the cone.

In this work, the conical spiral antenna is analyzed by using the FDTD method. The perfectly matched layer (PML) absorbing boundary condition truncates the open region surrounding the antenna. In the FDTD model, space is divided into cubic cells, and the perfectly conducting (PEC) arms of the conical spiral antenna are approximated by a staircased surface. Figure 12 (a) shows the FDTD mesh of this antenna, where the parameters are chosen as $D_1 = 2.5\text{mm}$, $D_2 = 7.5\text{mm}$, $\theta = 7.5^\circ$, $\alpha = 90^\circ$, $\delta = 90^\circ$. The design frequency bandwidth is 20GHz-40GHz. The antenna is fed by a transmission line. The Gaussian pulse current is used to launch a wide band frequencies source. The reflected current in the transmission line was Fourier transformed to frequency domain, and thus we can obtain the reflection coefficients, and

thus voltage standing wave ratio (VSWR), as shown in Fig.12 (b). From the figure, we may see that over a very wide band the VSWR are below 2.

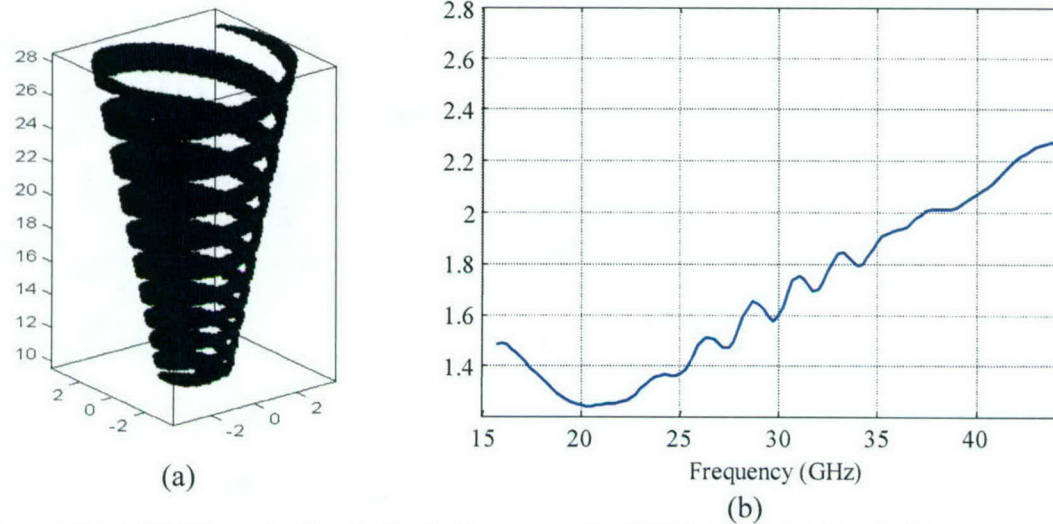


Figure 12. (a) FDTD mesh of conical spiral antenna, (b) VSWR plot within band of interest.

Once the near fields are known, the far fields can be propagated based on a near-to-far transformation. Figure 13 shows 3D radiation patterns at frequencies of 20GHz, 30GHz and 40GHz. At the center frequency the radiation pattern has a narrow beam width and small side lobe.

The directivity of a conical spiral antenna can be improved by reducing the angle θ_0 . However, it turns out that this increases difficulties in the fabrication of this kind antenna, particularly in the high frequency range. In addition, it is not compatible with our planar fabrication processes. Thus, in the following section we investigate the planar spiral antenna.

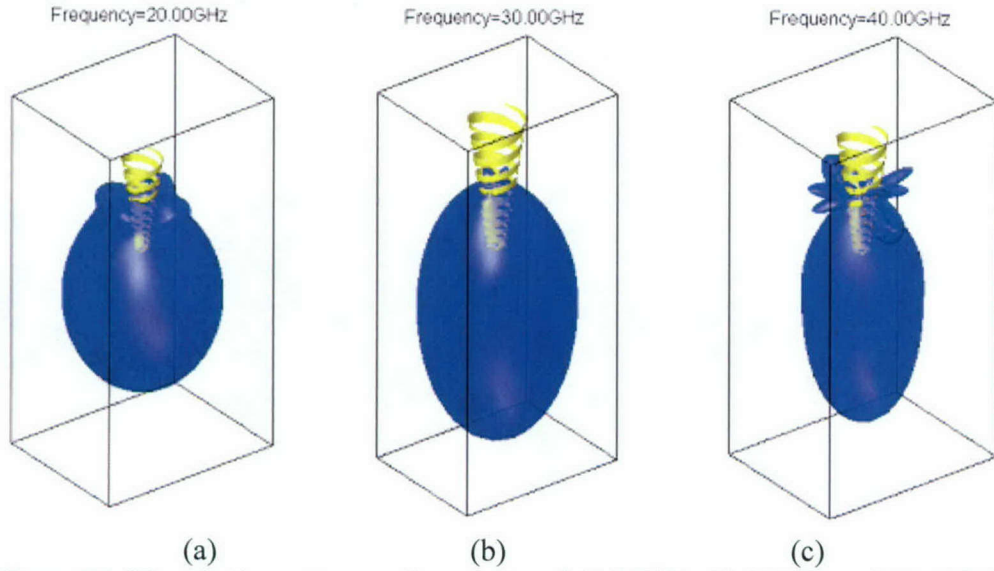


Figure 13. 3D radiation patterns at frequencies of (a) 20GHz, (b) 30GHz, and (c) 40GHz.

2.2.2. Two-arm Planar Spiral Antenna

As we mentioned in last section, while $\theta = 90^\circ$, the conical spiral antenna reduces to planar format, as shown in Fig. 14 (a). The antenna is defined by inner radius R_i , the width of strip s , the spacing between strips w , the thickness of strip h and the number of turns N . In this case we choose $s=w$.

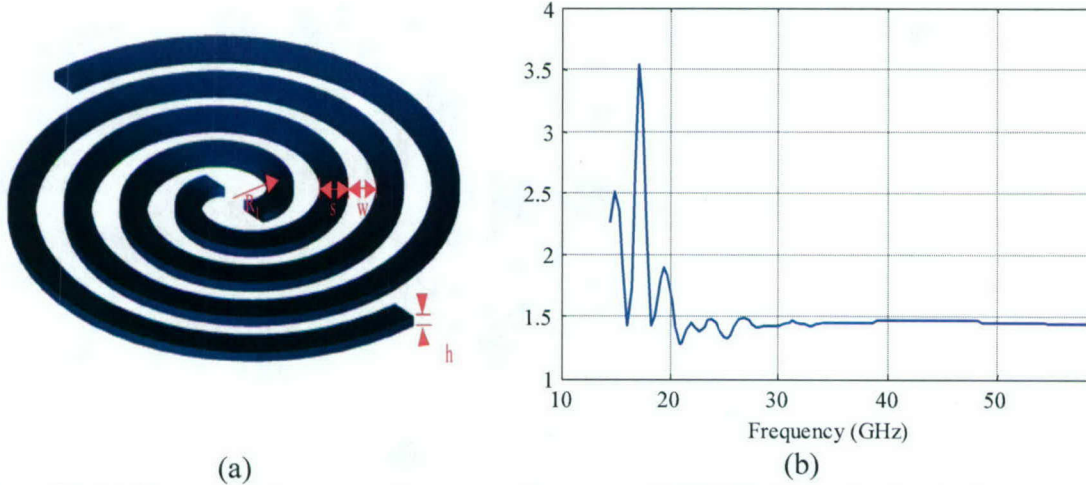


Figure 14. (a) Geometry of two-arm planar spiral antenna, (b) VSWR plot within band of interest.

We designed a planar spiral antenna, which operated within 20-40GHz. The design parameters are given by $R_i = s = w = 0.3\text{mm}$, and the thickness of strip is 0.05mm . The number of turns is chosen as $N = 4$. Figure 14 (b) shows the VSWR within frequency range 15-60GHz. From this figure we can observe that over a wide frequency range the VSWR is below 1.5, and thus demonstrates excellent frequency-independent of this antenna. In Figure 15 we show the 3D radiation patterns at frequencies of 20GHz, 30GHz, and 40GHz. This antenna radiates in both directions. However, it is easy to realize a single directivity of radiation pattern by including a cavity backed structure or a ground plane.

3. CONCLUSION

In this report, we have summarized our effort to develop and demonstrate the design, fabrication, and experimental characterization of the necessary components in a millimeter wave imaging system. We employed our electromagnetic modeling expertise and developed costumed in-house electromagnetic simulation codes to design and refine the system specifications. A novel two-element all-diffractive millimeter wave imaging system has been proposed. This design significantly reduces the overall size and weight of system while sufficiently meets and even exceeds the military mission specifications. Numerical results demonstrate that this designed system has high resolution and wide field of view up to $\pm 15^\circ$, and yet validate the high performance of this system. We also set up new and dedicated a mmW facility that included low- and high-end network analyzer, which encompasses a test and measurement capability spanning 45MHz through 110GHz. A new probe station, which includes 3D XYZ stage scanning system, various frequency probes as well as an antenna measurement system, has been built. The new test platform with capability of 3D near field scanning allows us fully characterize and simulate

mmW radiation. Based on this new mmW imaging test system, the in-house fabricated diffractive mmW lens has been characterized and obtained excellent results, which serve to demonstrate the capability for their use in a mmW system. In addition, we investigated two broadband frequency-independent antennas: conical and planar spiral antennas. Numerical electromagnetic tools were developed to analyze and design these antennas. Simulation results show great opportunity of these antennas to be integrated into the high sensitivity MMW detection systems.

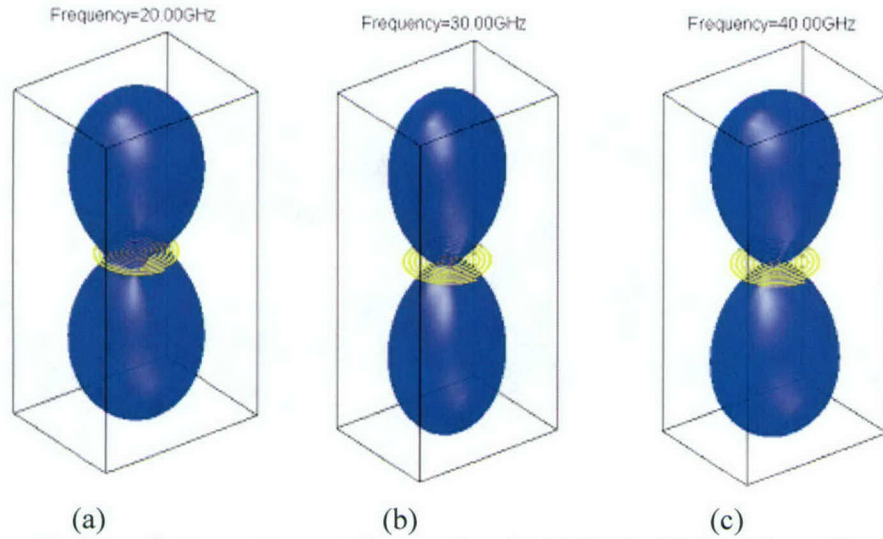


Figure 15. 3D radiation patterns at frequencies of (a) 20GHz, (b) 30GHz, and (c) 40GHz.